ELSEVIER

Nuclear Physics A681 (2001) 299c–308c

NUCLEAR PHYSICS A

www.elsevier.nl/locate/npe

Isospin Fractionation in Nuclear Fragmentation

G. Verde [a], H.S. Xu [a], T.X. Liu [a], X.D. Liu [a], W.G. Lynch [a], W.P. Tan [a], M.B. Tsang [a], A. VanderMolen [a], A. Wagner [a], H.F. Xi [a], C.K. Gelbke [a], L. Beaulieu [b], B. Davin [b], Y. Larochelle [b], T. Lefort [b], R.T. de Souza [b], R. Yanez [b], V. Viola [b], R.J. Charity [c], L.G. Sobotka [c]

[a]National Superconducting Cyclotron Laboratory and Department of Physics and Astronomy, Michigan State University, East Lansing, MI 48824, USA

[b]Department of Chemistry and IUCF, Indiana University, Bloomington, IN 47405, USA

[c]Department of Chemistry, Washington University, St. Luis, MO 63130, USA

Isotopic distributions for light particles and intermediate mass fragments have been measured for ^{112}Sn+^{112}Sn, ^{112}Sn+^{124}Sn, ^{124}Sn+^{112}Sn and ^{124}Sn+^{124}Sn collisions at E/A=50 MeV. Isotope, isotone and isobar yield ratio techniques are utilized to obtain an estimate of the relative abundance of free neutrons and protons at breakup. Consistent with the predictions of statistical models, which include two components in the liquid gas phase transition, neutrons and protons are not uniformly distributed at breakup. Instead, the neutron excess is amplified in the light charged particles.

1. Introduction

Nuclear matter is predicted to exhibit a phase transition between a Fermi liquid and a nucleonic gas at temperatures of the order of 5-15 MeV. Analyses of nuclear multifragmentation support the proposition that a region of mixed-phase may be formed in nuclear collisions [1–3]. The role of isospin in such processes has not been extensively investigated; nonetheless, isospin effects may be important [4–6]. For example, recent calculations of two component (neutron and proton) systems predict decreasing critical temperatures for systems of increasing neutron excess, reflecting the fact that a pure neutron liquid probably does not exist [4]. Moreover, the neutron to proton (N/Z) ratio of the gas phase in two component equilibrium calculations is significantly larger than that of the liquid phase [4–7]. in contrast to models of fast fragmentation for which the (N/Z) ratio is homogeneous throughout the system [8,9]. Similar equilibrium assumptions lead to predictions of very large (A$\simeq$1000) nuclei forming about protons residing within the neutron-rich gas [10] of the inner crust of a neutron star.

Some indications of an isospin fractionation were obtained from the isotopic distributions of light clusters that display a sensitivity to the overall N/Z ratio of the system [11–13]. Comparisons between the N/Z ratios within fragments and the N/Z ratios of nucleons and light clusters at breakup have been complicated, however, by the lack of isotopic resolution of most multifragment detection arrays. New isotopically resolved multifrag-

0375-9474/01/$ – see front matter
PII S0375-9474(00)00531-5

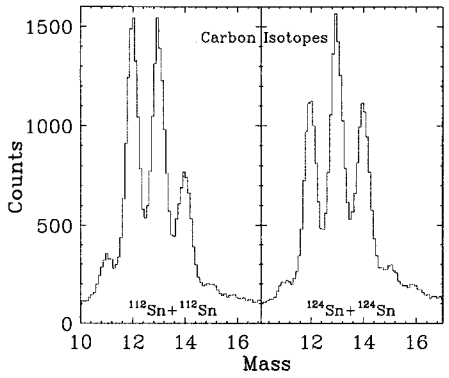

Figure 1. Carbon isotope particle identification histogram obtained for ^{112}Sn+^{112}Sn (left panel) and ^{124}Sn+^{124}Sn (right panel) reactions.

mentation measurements are presented in this article for systems of different overall N/Z ratio. Using appropriate isotope ratios, the ratio of the free neutron and proton densities at breakup can be extracted with little sensitivity to distortions from secondary decays of particle unstable nuclei. Within the context of the equilibrium assumption, the nucleonic gas is found to be neutron-enriched and the fragments more symmetric at breakup, in qualitative agreement with recent calculations of mixed phase equilibrium within two component lattice gas and mean field approaches [4–6].

2. Experimental details

To explore these issues, ^{112}Sn+^{112}Sn, ^{112}Sn+^{124}Sn, ^{124}Sn+^{112}Sn and ^{124}Sn+^{124}Sn collisions were studied by bombarding ^{112}Sn and ^{124}Sn targets of 5 mg/cm^2 areal density with 50 MeV per nucleon ^{112}Sn and ^{124}Sn beams from the K1200 cyclotron in the National Superconducting Cyclotron Laboratory at Michigan State University. Isotopically resolved particles with $1 \leq Z \leq 10$ were detected with nine telescopes of the Large Area Silicon Strip Array (LASSA) [14]. Each telescope consists of one 65μm single-sided silicon strip detector, one 500μm double-sided silicon strip detector and four 6-cm thick CsI(Tl) scintillators, read out by pin diodes. The 50mm x 50mm lateral dimensions of each LASSA telescope was divided by the strips of the silicon detectors into 256 ($\approx$3x3 mm^2) square pixels, providing an angular resolution of about $\pm 0.43^o$. The center of the LASSA device was located at a polar angle of $\theta = 32^o$ with respect to the beam axis, covering polar angles of $7^o \leq \theta \leq 58^o$. Impact parameter selection was provided by the multiplicity of charged particles [15] measured with LASSA and with 188 plastic scintillator - CsI(Tl) phoswich detectors of the Miniball/Miniwall array [16]. The combined apparatus covered 80% of the total solid angle. Central collisions were selected by gating on the top 4% of the charged-particle multiplicity distribution, corresponding to a reduced impact parameter

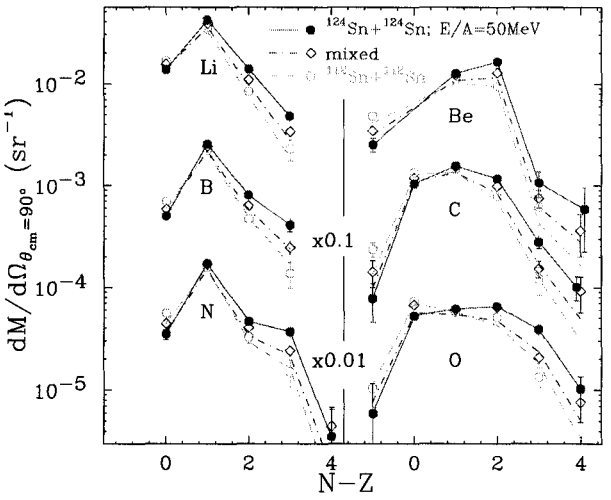

Figure 2. Isotopic distributions measured in central Sn+Sn collisions. See text for description.

of $b/b_{max} \leq 0.2$ in the sharp cut-off approximation [17]. Previous studies demonstrate that such collisions lead to bulk multifragmentation [18].

Figure 1 shows carbon-isotope particle-identification histograms [19], integrated over all LASSA telescopes for central ^{112}Sn+^{112}Sn (left panel) and ^{124}Sn+^{124}Sn (right panel) collisions. The isotopes from ^{11}C to ^{15}C are well resolved. The centroid of the mass distribution for the neutron-rich ^{124}Sn+^{124}Sn system is shifted by about 1/2 mass unit towards heavier isotopes compared to that for ^{112}Sn+^{112}Sn. The background in the spectrum arises from coincidence summing of signals from light particles and neutrons in the CsI(Tl) scintillators. For particles stopped in the Si detectors, the background is negligible [14].

3. Isotope yields and free nucleon densities

Isotopic distributions for Z=3-8 nuclei measured in central collisions and at intermediate rapidity ($0.4 \leq y/y_{beam} \leq 0.65$) are shown in Fig.2. The *mixed* label refers to the average between the cross sections measured in the intermediate N/Z systems ^{112}Sn+^{124}Sn and ^{124}Sn+^{112}Sn. The cross sections are plotted as a function of the "neutron excess" $N - Z$. As expected, a shift of the centroid of each distribution towards the neutron rich side is observed as one moves from the proton rich reaction system, ^{112}Sn+^{112}Sn, to the neutron rich one, ^{124}Sn+^{124}Sn. However, the observed isotopic effect in the yields is quite small: less than a factor of two. In order to investigate on the isotopic composition of the different phases and on possible fractionation phenomena, it is important to find other observables that are more sensitive to the isospin degree of freedom of the fragmenting system.

A basic framework for the extraction of free neutron and proton densities at breakup from isotopic ratios has been provided in ref. [6,20]. Assuming chemical equilibrium [20], one can write the primary multiplicity (before secondary decay of excited states) for an isotope with neutron number, N, and proton number, Z, in its i-th state as:

$$M_i(N,Z) \propto V \cdot e^{(N\mu_n + Z\mu_p + B(N,Z) - E_i^*)/T} \propto V \cdot \rho^N \cdot \rho^Z \cdot e^{B(N,Z)/T} \cdot e^{-E_i^*/T} \quad (1)$$

where V is the volume, $\rho_n = M_i(1,0)/V$ and $\rho_p = M_i(0,1)/V$ and are the primary free neutron and free proton densities respectively; $B(N,Z)$ and E_i^* are the ground state binding energy and excitation energy of the isotope in the i-th state; μ_n and μ_p are the neutron and proton chemical potentials and T is the temperature. Secondary decay of excited fragments after breakup introduces corrections to the final yields. The leading order correction arises from particle stable states and is a multiplicative factor, $\tilde{z}_{N,Z}(T) = \sum_{i,stable}(2J_i+1)\cdot e^{-E_i^*/T}$ where the sum is over particle stable states (with spin J_i) of the fragment. We further assume that the correction due to particle unstable decay can be represented by another multiplicative factor $f_{N,Z}(T)$:

$$M_{obs}(N,Z) \propto V \cdot \rho^N \cdot \rho^Z \cdot e^{B(N,Z)/T} \cdot \tilde{z}_{N,Z}(T) \cdot f_{N,Z}(T) \quad (2)$$

In principle, the influence of $\tilde{z}_{N,Z}(T)$ and $f_{N,Z}(T)$ can be assessed by model calculations. In order to investigate the isotopic composition of the different nuclear phases, it is important to find observables which maximize the sensitivity to isospin effects and minimize the sensitivity to temperature and sequential decays.

Single and double isotope and isotone ratios have been proposed to extract information about the temperature and the free neutron and proton densities at breakup [20]. Extensive studies indicate that distortions from sequential decays are specific to each ratio and depend less on entrance channel [21–23]. From Eq. 2, the multiplicity ratios of two isotopes differing by k neutrons is related to the free neutron density by:

$$\frac{M_{obs}(N+k,Z)}{M_{obs}(N,Z)} = \frac{\tilde{z}_{N+k,Z}(T)\cdot f_{N_k,Z}(T)}{\tilde{z}_{N,Z}(T)\cdot f_{N,Z}(T)} \cdot (\rho_n)^k \cdot e^{\Delta B/T}, \quad (3)$$

where $\Delta B = B(N+k,Z) - B(N,Z)$ is the binding energy difference between the two isotopes. The multiplicity ratios of two isotones differing by k protons is related to the free proton density by:

$$\frac{M_{obs}(N,Z+k)}{M_{obs}(N,Z)} = \frac{\tilde{z}_{N,Z+k}(T)\cdot f_{N,Z+k}(T)}{\tilde{z}_{N,Z}(T)\cdot f_{N,Z}(T)} \cdot (\rho_p)^k \cdot e^{\Delta B/T}, \quad (4)$$

where $\Delta B = B(N,Z+k) - B(N,Z)$ is the binding energy difference between the two isotones.

The ratio of the multiplicities of neighboring mirror nuclei is related to the ratio of the free neutron and proton densities by:

$$\frac{M_{obs}(Z,N)}{M_{obs}(N,Z)} = \frac{\tilde{z}_{Z,N}(T)\cdot f_{Z,N}(T)}{\tilde{z}_{N,Z}(T)\cdot f_{N,Z}(T)} \cdot \frac{\rho_n}{\rho_p} \cdot e^{\Delta B/T}, \quad (5)$$

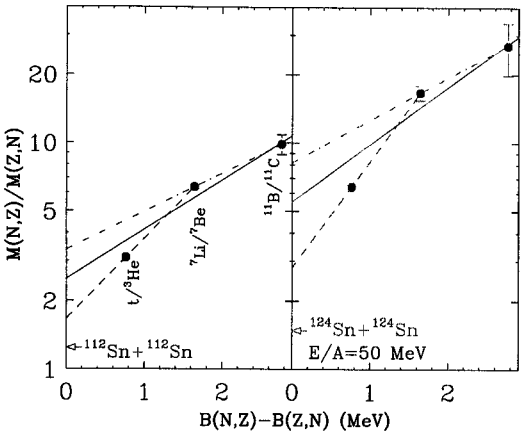

Figure 3. Isobar ratios for three mirror nuclei obtained from the ^{112}Sn+^{112}Sn (left panel) and ^{124}Sn+^{124}Sn (right panel) reactions. See text for explanation of the lines.

where $\Delta B = B(Z,N) - B(N,Z)$ is the binding energy difference between the two mirror nuclei and $N = Z - 1$. The similarity between the excited particle stable states of the two mirror nuclei leads to an approximate cancellation of the partition functions $\tilde{z}_{Z,N}(T)/\tilde{z}_{N,Z}(T) \simeq 1$, which should induce also a reduction of the secondary decay distortions in the obervable proposed in Eq. 5.

To estimate ρ_n/ρ_p using Eq. 5, three pairs of mirror nuclei, ^{3}H/^{3}He, ^{7}Li/^{7}Be and ^{11}C/^{11}B were analyzed for the ^{112}Sn+^{112}Sn and ^{124}Sn+^{124}Sn systems. The solid points in Fig. 3 show the isobaric yield ratios of these mirror nuclei as a function of the binding energy difference, ΔB. The data display a trend similar to Eq. 5, but differ in details, possibly due to Coulomb effects and the secondary decay factor $f_{Z,N}(T)/f_{N,Z}(T)$ which have been neglected. Assuming the correction to the individual ratios due to the secondary decay factor $f_{Z,N}(T)/f_{N,Z}(T)$ to be random and larger than the experimental uncertainties, extrapolating to vanishing ΔB via the solid lines yields values, following Eq. 5, for ρ_n/ρ_p of 2.5 for the ^{112}Sn+^{112}Sn system (left panel) and 5.5 for the ^{124}Sn+^{124}Sn system (right panel). Secondary decay calculations using SMM models [25,26], which do not reproduce the detail features of the isotopic distributions, predict that such extrapolations may underestimate ρ_n/ρ_p by as much as 30-50%. Alternative extrapolations, denoted by the dashed and dot-dashed lines, provide values for ρ_n/ρ_p which range from 1.7 to 3.4 for the ^{112}Sn+^{112}Sn system (left panel) and from 2.8 to 8.2 for the ^{124}Sn+^{124}Sn system (right panel). Statistical models with more accurate treatment of the sequential decay may reduce the uncertainties in these estimates. In all cases, the lower limits of these values are significantly larger than M(n)/M(p) =1.24 and 1.48 of the initial system marked by arrows in Fig. 3. This would suggest that the gas, consisting of free nucleons, contains proportionately more neutrons than the total system. The isobar ratios extracted for

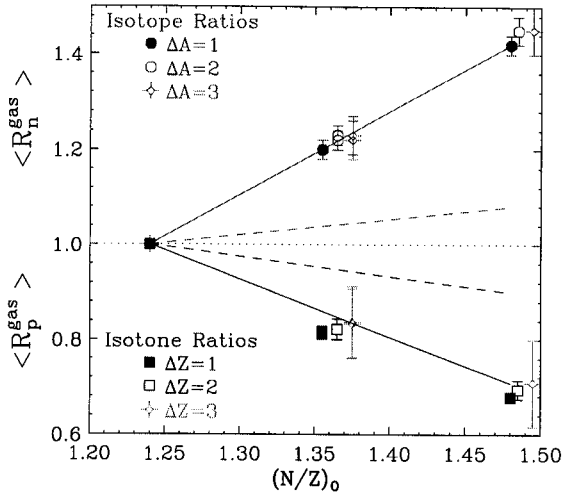

Figure 4. The mean relative free neutron and free proton densities (Eq. 6 and 7) as a function of $(N/Z)_0$. The solid and dot-dashed lines are the expected n-enrichment and p-depletion with the increase of isospin of the initial systems.

the mirror nuclei in the ^{124}Sn+^{124}Sn system is about a factor of 2 larger than the ratios measured in the ^{112}Sn+^{112}Sn system.

4. Results from relative isotope and isotone ratios

The absolute values of the ratios ρ_n/ρ_p, obtained from the mirror nuclei, are still affected by large uncertainties and observables which are less affected by secondary decay effects must be used to probe the neutron enhancement of the gas phase. Distortions from sequential decays can be further minimized by normalizing the isotopic and isotonic ratios in Eqs. 3 and 4, to those of the ^{112}Sn+^{112}Sn system, giving a relative free neutron density,

$$(\hat{\rho_n})^k = \frac{M_{obs}(N_i+k,Z_i)}{M_{obs}(N_i,Z_i)} \Big/ \frac{M^{112}_{obs}(N_i+k,Z_i)}{M^{112}_{obs}(N_i,Z_i)} = \left(\frac{\rho_n}{\rho_n^{112}}\right)^k, \tag{6}$$

and a relative free proton density,

$$(\hat{\rho_p})^k = \frac{M_{obs}(N_i,Z_i+k)}{M_{obs}(N_i,Z_i)} \Big/ \frac{M^{112}_{obs}(N_i,Z_i+k)}{M^{112}_{obs}(N_i,Z_i)} = \left(\frac{\rho_p}{\rho_p^{112}}\right)^k, \tag{7}$$

In these expressions, it has been assumed that temperature differences for the four systems (which have nearly the same center of mass energy per nucleon) are negligible [24], enabling the cancellations of both the binding energy factors and the partition functions. Cancellations of the particle unstable feeding corrections are also assumed [21–23].

Table 1
Relative free proton and neutron densities (Eq. 6 and 7) from two model calculations before and after sequential decays and from primary free proton and free neutron multiplicities.

$\hat{\rho}_n = \frac{M^{124}(n)/124}{M^{112}(n)/112}$	$\langle\hat{\rho}_n\rangle$(primary)	$\langle\hat{\rho}_n\rangle$(final)	Models [Ref.]
1.70	1.65±0.10	1.60±0.13	SMM1 [24]
1.71	1.79±0.06	1.72±0.18	SMM2 [25]
$\hat{\rho}_p = \frac{M^{124}(p)/124}{M^{112}(p)/112}$	$\langle\hat{\rho}_p\rangle$(primary)	$\langle\hat{\rho}_p\rangle$(final)	Models [Ref.]
0.50	0.49±0.03	0.60±0.15	SMM1 [24]
0.47	0.50±0.02	0.60±0.10	SMM2 [25]

To test these cancellations, we performed two different Statistical Multifragmentation Model (SMM) calculations [25,26], with A=248, Z=100 and A=224, Z=100, E*/A=5 MeV. The SMM calculations described in Ref. [25] utilize the available empirical levels and branching ratios for the secondary decay stage, while the calculations in Ref. [26] use parameterizations to calculate both. For simplicity, only k=1 isotope and isotone ratios are used to calculate the relative free n and p densities before and after sequential decay. Table 1 lists the mean relative free nucleon density, $\langle\hat{\rho}_n\rangle$ and $\langle\hat{\rho}_p\rangle$, before and after secondary decay. The spread of the distribution of ratios is indicated by the standard deviations in the Table 1 (The standard deviations of the calculations are typically 50% larger than those of the experiment). Values for $\hat{\rho}_n$ and $\hat{\rho}_p$, derived directly from the predicted primary free nucleon multiplicities, are also given. The mean values, $\langle\hat{\rho}_n\rangle$ and $\langle\hat{\rho}_p\rangle$, obtained from averaging ratios of either the primary or final multiplicities track these calculated relative free nucleon densities at breakup very well. This suggests that experimental values for $\langle\hat{\rho}_n\rangle$ and $\langle\hat{\rho}_p\rangle$ are robust with respect to distortions from sequential decay and can provide reasonable estimations for the actual relative free neutron and proton densities at breakup.

Experimental values for $\langle\hat{\rho}_n\rangle$ and $\langle\hat{\rho}_p\rangle$ were extracted for central collisions from isotope yields measured with good statistics and low background and listed in Table 2. To reduce the sensitivity to projectile and target remnants, these data were further selected by a rapidity gate of $0.4 \leq y/y_{beam} \leq 0.65$, where y and ybeam are the rapidities of the analyzed particle and beam, respectively.

The resulting mean values, $\langle\hat{\rho}_n\rangle$ and $\langle\hat{\rho}_p\rangle$, extracted from isotope ratios for the four systems ^{112}Sn+^{112}Sn, ^{112}Sn+^{124}Sn, ^{124}Sn+^{112}Sn, ^{124}Sn+^{124}Sn are shown in Fig. 4 as a function of the N/Z ratio for the composite system, $(N/Z)_O$. The solid circles and squares denote values for $\langle\hat{\rho}_n\rangle$ and $\langle\hat{\rho}_p\rangle$ extracted using Eq. 6 and 7 for k=1, the open circles and squares denote corresponding values for k=2 and the stars denote values for k=3. The error bars include both statistical errors, uncertainties arising from background subtraction and systematic errors. The excellent agreement between the extracted values obtained for k=1, 2 and 3 suggests that the factorization into neutron and proton densities in Eq. 1 and the cancellation of the secondary decay corrections in Eq. 6 and 7 are valid. The agreement between the mixed systems, ^{112}Sn(beam)+^{124}Sn(target) and ^{124}Sn(beam)+^{112}Sn(target), with $(N/Z)_O$=1.36 reflects the fact that the kinematic dis-

Table 2
List of isotope and isotone ratios used

Isotope Ratios			**Isotone Ratios**		
ΔA=1	ΔA=2	ΔA=3	ΔZ=1	ΔZ=2	ΔZ=3
d/p			^{3}He/d		
t/d	t/p		^{4}He/t		
^{4}He/^{3}He	^{6}He/^{4}He	^{6}He/^{3}He	^{7}Li/^{6}He		
^{7}Li/^{6}Li		^{7}Be/^{6}Li			
^{8}Li/^{7}Li	^{8}Li/^{6}Li		^{9}Be/^{8}Li		
^{9}Li/^{8}Li	^{9}Li/^{7}Li	^{9}Li/^{6}Li	^{10}B/^{9}Be	^{10}B/^{8}Li	
^{10}Be/^{9}Be	^{9}Be/^{7}Be	^{10}Be/^{7}Be	^{11}B/^{10}Be	^{11}B/^{9}Li	
^{11}B/^{10}B			^{12}C/^{11}B	^{12}C/^{10}Be	^{12}C/^{9}Li
^{12}B/^{11}B	^{12}B/^{10}B		^{13}C/^{12}B		
^{13}B/^{12}B	^{13}B/^{11}B	^{13}B/^{10}B	^{14}C/^{13}B		
^{13}C/^{12}C			^{14}N/^{13}C	^{14}N/^{12}B	
^{14}C/^{13}C	^{14}C/^{12}C		^{15}N/^{14}C	^{15}N/^{13}B	
^{15}N/^{14}N			^{16}O/^{15}N	^{16}O/^{14}C	^{16}O/^{13}B
^{16}N/^{15}N	^{16}N/^{14}N		^{17}O/^{16}N	^{17}O/^{15}C	
^{17}N/^{16}N	^{17}N/^{15}N	^{17}N/^{14}N	^{18}O/^{17}N		
^{17}O/^{16}O					
^{18}O/^{17}O	^{18}O/^{16}O				

tortions due to the acceptance of LASSA are negligible. If the relative concentrations of neutrons and protons were the same throughout each system and the overall nuclear matter density was independent of $(N/Z)_O$, the relative free neutron and proton densities as functions of $(N/Z)_O$ would follow the solid and dashed lines in Fig. 4, respectively. The experimental data shows that as $(N/Z)_O$ increases, the system responds by making the asymmetry of the gas (given by the ratio $\langle\hat{\rho}_n\rangle/\langle\hat{\rho}_p\rangle$) much greater than the asymmetry of the total system (given by the ratio of solid to dashed lines). The results obtained from isotope and isotone ratios are in agreement with the ones extracted from mirror nuclei ratios, shown in Fig. 3. Both the analyses shown in Figs. 3 and 4 indicate a neutron enhancement for the neutron rich system that is roughly twice that of the neutron deficient system.

Within the same statistical assumptions of Eq. 1-7, distortions from sequential decays can be minimized also by normalizing each of the isotopic yields in Eq. 2 for the ^{124}Sn+^{124}Sn system to that of the ^{112}Sn+^{112}Sn system,

$$\frac{M^{124}_{obs}(N_i,Z_i)}{M^{112}_{obs}(N_i,Z_i)} = C\cdot\left(\frac{\rho_p^{124}}{\rho_p^{112}}\right)^{Z}\cdot\left(\frac{\rho_n^{124}}{\rho_n^{112}}\right)^{N} = C\cdot(\hat{\rho}_p)^{Z}\cdot(\hat{\rho}_n)^{N} \tag{8}$$

In Fig. 5 the measured relative isotope (upper panel) and isotone (lower panel) ratios $Y^{124}(N_i,Z_i)/Y^{112}(N_i,Z_i)$ (data points) are plotted for Z=3-8. Ratios calculated using Eq. 8 and the values of $\langle\hat{\rho}_n\rangle$=1.42 and $\langle\hat{\rho}_p\rangle$=0.68 (from Fig. 4) are shown as dot-dashed lines. These calculations are normalized to the experimental values of ^{7}Li. The excellent

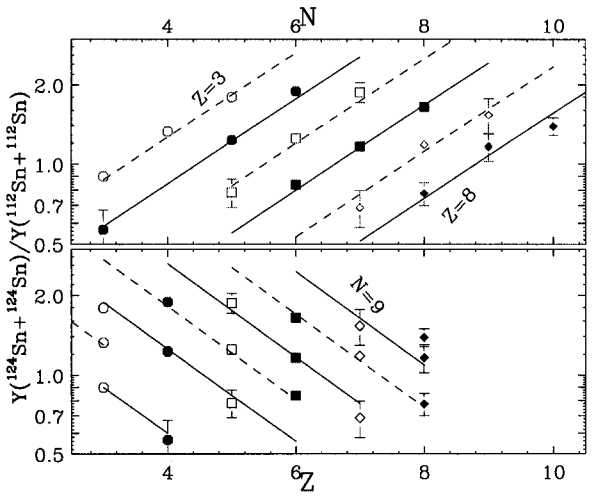

Figure 5. Measured (data points) and predicted (lines) relative isotope (upper panel) and isotone (lower panel) ratios of Eq. 8.

agreement between the data and the predictions of Eq. 8, suggest that the proposed statistical assumptions and the cancellation of secondary decay corrections in the used observables are valid.

5. Summary

Isotope distributions from Z=1 to Z=8 particles emitted in four different Sn+Sn ractions ranging from initial isospin of 1.24 to 1.48, by using the multidetector array LASSA. In the framework of a grandcanonical statistical approach, the isotopic composition of the nuclear liquid and gas phases has been studied using observables which exhibit small distortions from sequential decays. The nucleon density extracted using isotope, isotone and isobar ratios suggest that the gas phase is more neutron enriched that the liquid phase represented by bound nuclei, consistent with the predicted partial fractionation of nucleon components in the liquid gas phase transition. The observed effects are significantly enhanced in neutron-rich systems relative to neutron-deficient systems. The extracted results suggest also a systematics of isotope and isotone distributions which can extended to other systems and reaction mechanisms [27].

REFERENCES

1. A.S. Botvina, I.N. Mishustin, and M. Begemann-Blaich, Nucl. Phys. A 584, 737 (1995).
2. B.A. Li, A.R. De Angelis, and D.H.E. Gross, Phys.Lett.B 303, 225 (1993).
3. M. D'Agostino et al., Phys. Lett. B 371, 175 (1996).

4. H. Mller and B. D. Serot, Phys. Rev. C 52, 2072 (1995).
5. Ph. Chomaz and F. Gulminelli, Phys. Lett. B 447, 221 (1999). J. Pan and S. Das Gupta, Phys. Rev. C 57, 1839 (1998).
6. J. Randrup and S.E. Koonin, Nucl. Phys. A 356, 223 (1981).
7. It may be possible for the free proton density to exceed the free neutron density in extremely proton rich systems.
8. J. Aichelin, J. Hufner and R. Ibarra, Phys. Rev. C 30, 107 (1984).
9. W. Bauer, D.R. Dean, U. Mosel and U. Post, Phys. Lett. B 150, 53 (1985).
10. C. J. Pethick and D. G. Ravenhall, Ann. Rev. Nucl. Part. Sci. 45, 429 (1995).
11. J. F. Dempsey et al., Phys. Rev, C 54, 1710 (1996).
12. L. G. Sobotka et al., Phys. Rev. C 55, 2109 (1997).
13. R. Laforest et al., Phys. Rev. C59 (1999) 2567 and refs. therein.
14. A. Wagner et al., NSCL Preprint MSUCL-1150 and to be published
15. L. Phair et al., Nucl. Phys. A 548, 489 (1992).
16. R.T. de Souza et al., Nucl. Instrum. Methods A 295, 109 (1990). The Miniwall, a granular extension of the Miniball to forward angles, uses the readout technology of D.W. Stracener et al., Nucl. Instrum. Methods A 294, 485 (1990).
17. C. Cavata et al., Phys. Rev. C42, 1760 (1990); Y.D. Kim et al., Phys. Rev. C 45, 338 (1992).
18. G. J. Kunde, et al., Phys. Rev. Lett. 77, 2897 (1996).
19. T. Shimoda, M. Ishihara, K. Nagatani, and T. Nomura, Nucl. Instr. and Methods 165, 261 (1979).
20. S. Albergo et al., Nuovo Cimento A 89, 1 (1985).
21. M. B. Tsang, W. G. Lynch, and H. Xi W. A. Friedman, Phys. Rev. Lett. 78, 3836 (1997).
22. H. Xi et al., Phys. Rev. C 59, 1567 (1999); H. Xi et al., Phys. Lett B 431, 8 (1998).
23. V. Viola, K. Kwiatkowski, and W.A. Friedman, Phys. Rev. C 59, 2660 (1999)
24. G.J. Kunde et al., Phys. Lett. B 416, 56 (1998).
25. A.S. Botvina et al., Nucl. Phys. A475, 663 (1987); J.P. Bondorf et al., Phys. Rep. 257, 133 (1995)
26. W. Tan, private communication and to be published.
27. M.B. Tsang et al., present prodeedings.